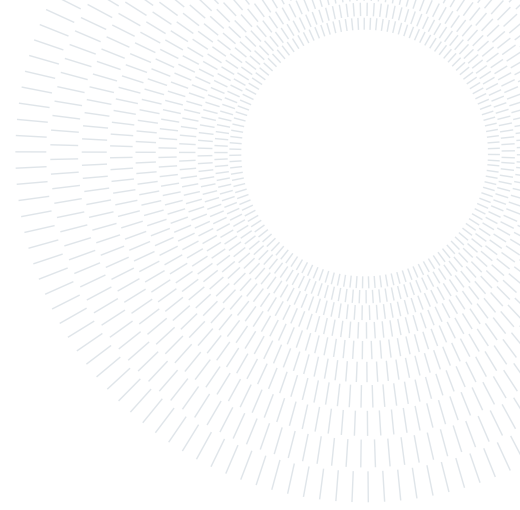




POLITECNICO
MILANO 1863

SCUOLA DI INGEGNERIA INDUSTRIALE
E DELL'INFORMAZIONE



Adjoint-based data assimilation of a compressible starting jet

TESI DI LAUREA MAGISTRALE IN

AERONAUTICAL ENGINEERING - INGEGNERIA AERONAUTICA

Riccardo Consonni, 10572121

Advisor:

Prof. Maurizio Quadrio

Co-advisors:

Prof. Jörn Sesterhenn
Hamam Mohamed

Academic year:

2022-2023

Abstract: An observation analysis of the adjoint-based data assimilation (DA) method applied to a compressible starting jet is performed. First, the adjoint-based data assimilation framework is derived and validated for a simple acoustic source identification problem. Second, an observation analysis on the Kovasznay modes is done with the intention of having a benchmark for the observational properties of the derived DA framework applied to perturbations around a base state. Third the data assimilation of a compressible starting jet is presented. The data for the assimilation is taken from a DNS and is used as synthetic experimental input. The ability of the data assimilation procedure of finding a good fit given two snapshots of the flow at different timesteps is evaluated. Furthermore, a systematic observability analysis is also performed in the starting jet case. The capability of the data assimilation framework of fitting the available data is positively evaluated. The particular case of application used in this work presented difficulties in reconstructing unknown variables.

Key-words: data assimilation, compressible flow, starting jet, adjoint Navier-Stokes equations

1. Introduction

In the study of complex fluid mechanics problems, observational data and fluid simulations are used side-by-side and are compared, in the post-processing phase, to find an underlying explanation for the fluid phenomena in question. However the experiments and simulations rarely provide perfectly matching results and their interaction is often limited to a simple comparison of the data.

Experiments provide us real-world data, which is generally what we want to study and predict. However the measurements are often corrupted by noise, and are often not exhaustive. In fact, it is not always easy, or possible, to access certain observables of the flow, i.e. entropy field. Moreover measuring instruments can be intrusive and modify the flow of interest in major ways.

Fluid simulations on the other hand give us complete information about the state and observables of the flow in every point of the domain, without any form of uncertainty due to noise or measuring equipment. The quality of the data depends on the underlying modelling assumptions and space-time discretization used to simulate the flow, which often lead to equations whose numerical solution can be computationally expensive to find. In turbulent flow, the uncertainty of initial and boundary conditions can also affect the correctness of simulations in a crucial way.

In the middle of these two paradigms data assimilation (DA) emerges as a natural and effective tool to synthesize the information of both model and experimental data in an optimal way. Data assimilation techniques integrate

optimally observational data with mathematical models to estimate the state of a system, thereby refining predictions and reducing uncertainties.

Data assimilation techniques found a lot of applications in many fields, e.g. meteorology [2], weather forecasting [22], control engineering, medical applications [6] and currently it's gaining popularity in fluid mechanics. Two main approaches can be identified [1]: a stochastic and a variational approach. The former makes use of stochastic filtering and estimation techniques such as *Best Linear Unbiased Estimator (least squares estimation)*, *Kalman filters* [12] [4] and nonlinear filtering methods [21]. The latter minimizes a loss function to find the model solution that best approximates the measurement data. For the computation of gradients an adjoint formulation is used. Popular methods are 3DVar and 4DVar. There are also many hybrid methods, that use both variational and stochastic methods [11] [20].

Both the approaches can be successfully used for the application of compressible fluid mechanics. In this thesis variational techniques will be used, as it has many advantages over stochastic approaches. It takes into account all of the experimental data simultaneously, and doesn't use any statistical models. Furthermore, adjoint formulations can be used for other purposes, like active flow control, order model reduction and sensitivity analysis. Furthermore, the research group in which this worked is developed has a lot of experience with adjoint-based techniques with application to compressible flows [25] [26] [15].

1.1. Objectives

There are multiple objectives for this thesis. First, a data assimilation framework is developed for the compressible Navier-Stokes equations and it is tested. This part will be reported in third section of this thesis.

Second, the data assimilation framework is going to be applied to the Kovasznay modes [13]. From this, an observation analysis is conducted with the goal of understanding the capabilities of the derived framework to reconstruct non-accessible fields from measured ones in the case of a perturbed condition from a base flow. An example is reconstructing the pressure field from the velocity vector field (or a PIV measurement). This task is particularly hard for compressible flows, since the pressure field is not identified completely by the velocity field like in the incompressible case, but there is also a thermodynamic component which must be considered. This part is reported in the fourth section of the thesis.

Third, the data assimilation of the compressible starting jet, made using a direct numerical simulation, is done and its observational capabilities are assessed. A systematic study is conducted with reference to possible experimental measurements that can be done at the research group's laboratory in the future. Similarly to the Kovasznay modes analysis, the capability of the data assimilation to infer unknown flow variables from measured ones will be assessed in the case of a compressible starting jet, the results are analyzed also through the lens of the Kovasznay modes analysis. Furthermore, the capability of finding a satisfying fit solution given two snapshots of experimental data in distant time steps is evaluated by comparing the found solution with the ground truth in the time step in between the two given snapshots. This breakdown is conducted in the fifth section of the thesis.

The investigation and the data assimilation setup is done taking into consideration the laboratory equipment present in the research group. This is because this work is a first step towards the ultimate goal of doing a fully data-driven DNS of a compressible starting jet using limited experimental measured data. This goal is a long term research project of the chair in which this work is developed.

A small part of the thesis is allocated to the direct numerical simulation of the compressible starting jet. It is worth mentioning that this thesis also included working on developing the direct numerical solver for compressible starting jets, in particular the implementation of the boundary conditions.

2. Numerical model for compressible jets

In this chapter the mathematical and numerical models for the compressible jet simulations will be indicated and explained. These types of flows are very complex, and due to turbulence, the physical processes that characterize these phenomena are of very different time and length scale. For this reason the choice of grid spacing is crucial for Direct Numerical Simulations (DNS). If the grid is not fine enough the small scales can't be resolved and the turbulent kinetic energy doesn't get dissipated, which causes instabilities and inaccurate results. However a very fine grid implies a very large computation, that might not be feasible depending on the computing resources one might have.

For flow simulation the CuNSF code is used. This is an in-house code developed in Julia and CUDA, as it is designed to run on GPU. The CuNSF solver is a porting of the already existing Fortran code (NSF) which has been continuously developed at Prof. Sesterhenn's group and validated in several studies.

2.1. Equations of motion

The motion of an unsteady fluid flow is governed by the Navier-Stokes Equations (NSE). Compressible NSEs are a set of highly nonlinear conservation laws, and they describe the motion of a fluid, in this case modeled as a Newtonian fluid, by imposing conservation of mass, momentum and energy. These equations must be closed using some thermodynamic relations.

These equations are highly coupled, but by following Kovasznay [13] argument, it is possible, using linearization, to decouple them into a set of linear PDEs that describe the perturbation of the state from a prescribed base-flow. These three equations are called *Kovasznay modes*: Acoustic mode (described by pressure perturbation), vorticity mode and entropy mode. These modes will be later used to conduct an observation analysis for the data assimilation framework, therefore the NSE are written using pressure, velocity and entropy in non-conservative form:

$$\begin{cases} \frac{\partial p}{\partial t} + u_i \frac{\partial p}{\partial x_i} = -\gamma p \frac{\partial u_i}{\partial x_i} + \frac{p}{c_v} \left(\frac{\partial s}{\partial t} + u_i \frac{\partial s}{\partial x_i} \right) & (1a) \\ \frac{\partial u_i}{\partial t} + u_j \frac{\partial u_i}{\partial x_j} = -\frac{1}{\rho} \frac{\partial p}{\partial x_i} + \frac{1}{\rho} \frac{\partial \tau_{ij}}{\partial x_j} & (1b) \\ \frac{\partial s}{\partial t} + u_i \frac{\partial s}{\partial x_i} = \frac{1}{\rho T} \left[-\frac{\partial}{\partial x_i} \left(-\lambda \frac{\partial T}{\partial x_i} \right) + \Phi \right], & (1c) \end{cases}$$

with:

$$\tau_{ij} := 2\mu \left(s_{ij} - \frac{1}{3} s_{kk} \delta_{ij} \right) \quad (2)$$

$$s_{ij} := \frac{1}{2} \left(\frac{\partial u_i}{\partial x_j} + \frac{\partial u_j}{\partial x_i} \right) \quad (3)$$

$$\Phi := \tau_{ij} s_{ij}. \quad (4)$$

The effects of bulk viscosity are neglected. To close the above equations we make the following thermodynamic hypothesis: the fluid is modeled by an ideal gas with gas constant $R = 287 \text{ m}^2/\text{K}/\text{s}^2$ and the viscosity is modeled with Sutherland's law [30]

$$p = \rho RT \quad (5)$$

$$\mu = \mu_0 \frac{T_0 + S}{T + S} \left(\frac{T}{T_0} \right)^{3/2} \quad (6)$$

using the following constants: $S = 110.4 \text{ K}$ (Sutherland's temperature), and T_0 and μ_0 the total temperature and the corresponding viscosity, respectively. Heat conductivity is, following Fourier's law, function of the viscosity:

$$\lambda = \mu \frac{c_p}{Pr} \quad (7)$$

with $\gamma = c_p/c_v = 1.4$, $c_p - c_v = R$ and $Pr = 0.71$ the Prandtl number.

2.2. Characteristic formulation and space-time discretization

The Navier-Stokes equations (1) can be rewritten in a characteristic wave formulation [27] as:

$$\begin{aligned} \frac{\partial p}{\partial t} = & -\frac{\rho c}{2} [(X^+ + X^-) + (Y^+ + Y^-) + (Z^+ + Z^-)] + \\ & + \frac{p}{c_v} \left(\frac{\partial s}{\partial t} + X^s + Y^s + Z^s \right) \end{aligned} \quad (8a)$$

$$\frac{\partial u}{\partial t} = - \left[\frac{1}{2} (X^+ - X^-) + Y^u + Z^u \right] + \frac{1}{\rho} \frac{\partial \tau_{1j}}{\partial x_j} \quad (8b)$$

$$\frac{\partial v}{\partial t} = - \left[X^v + \frac{1}{2} (Y^+ - Y^-) + Z^v \right] + \frac{1}{\rho} \frac{\partial \tau_{2j}}{\partial x_j} \quad (8c)$$

$$\frac{\partial w}{\partial t} = - \left[X^w + Y^w + \frac{1}{2} (Z^+ - Z^-) \right] + \frac{1}{\rho} \frac{\partial \tau_{3j}}{\partial x_j} \quad (8d)$$

$$\frac{\partial s}{\partial t} = - (X^s + Y^s + Z^s) + \frac{R}{p} \left[-\frac{\partial}{\partial x_i} \left(-\lambda \frac{\partial T}{\partial x_i} \right) + \Phi \right] \quad (8e)$$

with the following abbreviations:

$$\begin{aligned} X^\pm & := (u \pm c) \left(\frac{1}{\rho c} \frac{\partial p}{\partial x} \pm \frac{\partial u}{\partial x} \right) \\ Y^\pm & := (v \pm c) \left(\frac{1}{\rho c} \frac{\partial p}{\partial y} \pm \frac{\partial v}{\partial y} \right) \\ Z^\pm & := (w \pm c) \left(\frac{1}{\rho c} \frac{\partial p}{\partial z} \pm \frac{\partial w}{\partial z} \right) \\ X^v & := u \frac{\partial v}{\partial x}, \quad X^w := u \frac{\partial w}{\partial x}, \quad X^s := u \frac{\partial s}{\partial x} \\ Y^u & := v \frac{\partial u}{\partial y}, \quad Y^w := v \frac{\partial w}{\partial y}, \quad Y^s := v \frac{\partial s}{\partial y} \\ Z^u & := w \frac{\partial u}{\partial z}, \quad Z^v := w \frac{\partial v}{\partial z}, \quad Z^s := w \frac{\partial s}{\partial z}. \end{aligned} \quad (9)$$

This formulation has many advantages: a) High order of accuracy can be easily obtained, also at the boundaries. b) The boundary treatment is consistent with the interior scheme, this makes the implementation of non-reflecting boundary conditions simple, other boundary conditions like solid walls can be written in a similar way. c) This formulation is well-suited for massive parallelization. The above equations are valid for Cartesian coordinates only. It is possible to generalize them for curvilinear grids [27].

For the DNS of the compressible starting jet a central finite difference scheme will be employed, as it provides highly accurate approximations of derivatives, it is particularly efficient on structured grids and it's less dissipative than standard upwind and downwind methods. For the time advancing scheme an explicit fourth order Runge-Kutta method is used as it is very accurate and stable for reasonably small timesteps.

2.3. Computational domain and boundary conditions

For the jet simulations, a two-dimensional Cartesian domain is used; such geometry has four boundaries. The size of the domain is $10D \times 10D$ where D is the diameter of the inlet. On the left boundary a wall and inlet condition is imposed, while on all the other sides the boundary is imposed as non-reflective. The inlet center line is placed exactly on the centerline of the wall. On the opposite side of the inlet wall a sponge layer is used. For a more thorough discussion on the sponge layer see [3].

The unbounded chamber in which the jet computations take place is connected to a reservoir under pressure through a nozzle, as it can be seen in figure 1. What happens is that at time $t = 0$ an ideal membrane opens, and the fluid start flowing from the reservoir to the unbounded chamber.

To describe the behavior of the reservoir and the nozzle a simple one dimensional isentropic model used to compute the total pressure at the jet exit.

2.3.1 Non-reflecting BC

To have a precise simulation of acoustic phenomena it's important that the boundary conditions don't reflect outgoing acoustic waves. The implementation of these in-/outflow conditions generally consists of decomposing the flow in characteristic waves and setting the in-going wave to zero, and then recompute the waves into flow

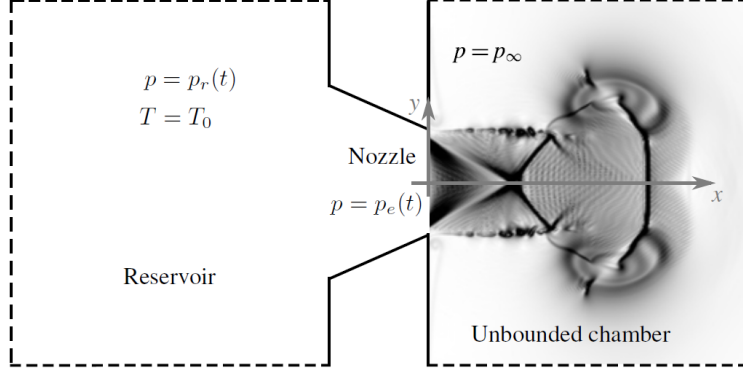


Figure 1: Compressible starting jet setup. p_r is the total pressure in the reservoir. p_∞ is the ambient pressure and p_e is the exit pressure. T_0 is the total temperature in the reservoir. Image taken from [5].

variables. However, in the present characteristic formulation this is not necessary as the flow variables are already decomposed into waves, therefore the implementation becomes straightforward. For the top boundary, normal to the y-axis the conditions are:

$$Y^u = Y^s = Y^- = 0. \quad (10)$$

For the other boundaries the formulation is analogous.

2.3.2 Wall with subsonic inlet

The following is a set of equations, written for a Cartesian grid, to consistently describe an isothermal boundary wall with a subsonic inlet [31] [5]. Let's consider equations 8, on the left boundary X^v can be set by imposing $\frac{\partial v}{\partial t} = 0$ on the wall (part of the no-slip condition) and inlet (horizontal jet). The thermodynamic relation for temperature is now introduced:

$$\frac{\partial T}{\partial t} = \frac{\partial T}{\partial p} \frac{\partial p}{\partial t} + \frac{\partial T}{\partial s} \frac{\partial s}{\partial t} = \frac{1}{\rho c_p} \frac{\partial p}{\partial t} + \frac{T}{c_p} \frac{\partial s}{\partial t}. \quad (11)$$

The set of four equations 8a, 8b, 8e, 11, has six unknowns $\frac{\partial p}{\partial t}$, $\frac{\partial u}{\partial t}$, $\frac{\partial s}{\partial t}$, $\frac{\partial T}{\partial t}$, X^+ , X^s ($\frac{\partial v}{\partial t}$ is already set). Specifying $\frac{\partial u}{\partial t}$ and $\frac{\partial T}{\partial t}$ delivers the equations that describe the flow behavior on the boundary:

$$X^v = \frac{\partial v}{\partial t} - \frac{1}{2} (Y^+ - Y^-) + \frac{1}{\rho} \frac{\partial \tau_{2j}}{\partial x_j} \quad (12a)$$

$$X^+ = X^- - 2 \frac{\partial u}{\partial t} + \frac{2}{\rho} \frac{\partial \tau_{1j}}{\partial x_j} - 2Y^u \quad (12b)$$

$$X^s = -\frac{c}{2T} (X^+ + X^- + Y^+ + Y^-) + \frac{\gamma}{\rho T} \left[-\frac{\partial}{\partial x_i} \left(-\lambda \frac{\partial T}{\partial x_i} \right) + \Phi \right] - \frac{c_p}{T} \frac{\partial T}{\partial t} - Y^s. \quad (12c)$$

At the wall $\frac{\partial u}{\partial t}$ and $\frac{\partial v}{\partial t}$ are set to zero (no-slip condition), just like the initial condition. The wall is isothermal, therefore $\frac{\partial T}{\partial t}$ is also set to zero. At the inlet the derivatives of u and T are set in such a way [5] [24] that pressure follows time evolution:

$$p_e(t^*) = p_\infty + (p_0 - p_\infty) \exp \left[\frac{-t^*}{C} \right] \tanh(Kt^*), \quad (13)$$

where $t^* = tU/D$ is the dimensionless time, U and D are the fully expanded velocity of the jet and inlet diameter. The constant C controls the rate of decay of the jet and K controls the impulsive stage of the jet. When C is increased, the decay becomes slower, when K is increased the impulsivity of the first stage is also increased [5]. The constant p_0 controls the amplitude of the exit pressure at the nozzle and it is related to $p_r(t=0)$.

The distinction between wall and inlet is made by building the space distribution of $\frac{\partial u}{\partial t}$ and $\frac{\partial T}{\partial t}$ using a function of the type:

$$f = \frac{1}{2} - \frac{1}{2} \tanh \left\{ 2\pi \left[r - \frac{1}{2} (D - \delta_w) \right] / \delta_w \right\}, \quad (14)$$

where r is the distance from the inlet centerline and δ_w is the shear layer thickness. In this way the time derivatives are set to zero on the wall and are set to the correct value on the inlet. The smooth transition between wall and nozzle is necessary to avoid numerical instabilities.

3. Adjoint-based data assimilation

In this section the adjoint-based data assimilation framework will be derived. First the concept of adjoint equations will be presented, then they will be derived for our fully compressible Navier-Stokes model in the continuous case and the necessary boundary conditions will be discussed. Optimization of the loss function will be gradient based, and therefore these equations will be very important, as their solutions give access to the gradient of the loss function with respect to the control variables one wants to use. In the end the data assimilation method will be presented, together with the possible optimization strategies that can be employed to find the minimum of the objective function. A simple case is presented as validation, showing the efficacy of the adjoint method for data assimilation tasks. The following derivations are based on the data assimilation framework developed in Prof. Sesterhenn's group, and they are mainly developed in [14].

3.1. Adjoint approach

In this section the adjoint equations will be introduced in the discrete case for the sake of simplicity, the derivation is based on [7]. The adjoint Navier-Stokes equations will be derived in 3.2 in a continuous form. To define the adjoint equations it is necessary to consider an objective function J . In this case it will be defined as product between a geometric weight \mathbf{g} and the system state \mathbf{q} .

$$J = \mathbf{g}^\top \mathbf{q}, \quad \mathbf{g}, \mathbf{q} \in \mathbb{R}^n. \quad (15)$$

The system state is the solution of:

$$\mathbf{A}\mathbf{q} = \mathbf{f}, \quad \mathbf{A} \in \mathbb{R}^{n \times n}, \mathbf{f} \in \mathbb{R}^n. \quad (16)$$

with \mathbf{A} as governing operator and \mathbf{f} the source term. To optimize J with respect too f it is necessary to solve the system 16 for many times for every different \mathbf{f} . To reduce the computational effort the adjoint equations are introduced

$$\mathbf{A}^\top \mathbf{q}^* = \mathbf{g}, \quad (17)$$

where \mathbf{q}^* is the adjoint variable. It is possible to rewrite J as an explicit function of \mathbf{f}

$$J = \mathbf{g}^\top \mathbf{q} = (\mathbf{A}^\top \mathbf{q}^*)^\top \mathbf{q} = \mathbf{q}^{*\top} \mathbf{A}\mathbf{q} = \mathbf{q}^{*\top} \mathbf{f}. \quad (18)$$

This expression enables the computation of J without the need of solving a linear system for every \mathbf{f} . This also allows an efficient determination of global effects of different forcings.

In the case of a nonlinear objective function J it is possible to linearize the problem around a base state $\mathbf{q} = \mathbf{q}_0 + \delta\mathbf{q}$

$$J + \delta J = \mathbf{g}^\top (\mathbf{q}_0 + \delta\mathbf{q}) \quad (19)$$

since the base state is a solution of the considered system the problem can be reformulated considering the expression

$$\delta J = \mathbf{g}^\top \delta\mathbf{q} \quad (20)$$

where the variation of the state $\delta\mathbf{q}$ is the solution of the problem $\mathbf{A}\delta\mathbf{q} = \delta\mathbf{f}$. The rest of the derivation for the adjoint equations in the nonlinear case becomes analogous to the above derivation.

3.2. Adjoint Navier-Stokes equations

The adjoint Navier stokes equations will now be derived in continuous form. For sake of simplicity the derivation will be made in a one dimensional setting, the generalization to the multidimensional case is straightforward. First let's introduce the set of equations 1 written in matrix form:

$$\partial_t \mathbf{q} + \mathbf{X}(\mathbf{q})\partial_x \mathbf{q} + \mathbf{F} = \mathbf{f}, \quad (21)$$

where the terms in the equation are defined as:

$$\mathbf{X}(\mathbf{q}) = \begin{bmatrix} u & \gamma p & 0 \\ 1/\rho & u & 0 \\ 0 & 0 & u \end{bmatrix} \quad (22)$$

$$\mathbf{F} = \begin{bmatrix} -\frac{p}{c_v} \left(\frac{\partial s}{\partial t} + u \frac{\partial s}{\partial x} \right) \\ -\frac{1}{\rho} \partial_x \tau_{11} \\ -\frac{R}{p} [\partial_x (\lambda \partial_x T) + \Phi] \end{bmatrix},$$

and \mathbf{f} is a generic forcing term and $\mathbf{q} = (p, u, s)^\top$ is the state vector. This form of the equations will be very handy for the following computations.

The adjoint equations arises from the definition of a functional to be minimized, the functional that will be used for the derivation will have the following form:

$$J = \int_V \int_{t_0}^T g(\mathbf{q}) dV dt, \quad (23)$$

where g is a generic nonlinear function. The function is integrated over the the space domain V and time span $[t_0, T]$ defined by the specific problem at hand. To find the adjoint equation the functional must be augmented by using a Lagrange multiplier \mathbf{q}^* multiplied by 21, this addition is allowed as we are adding a term that is equal to zero. From now on the derivation will be done in index form:

$$J = \iiint g(q_\alpha) dV dt - \iiint q_\alpha^* [\partial_t q_\alpha + X_{\alpha\beta} \partial_x q_\beta + F_\alpha - f_\alpha] dV dt. \quad (24)$$

To compute the sensitivity of the functional with respect to a variable, in this case with respect to the forcing term, it is necessary to perturb the functional by taking the first variation δJ .

$$\delta J = \iiint \frac{\partial g}{\partial q_\alpha} \delta q_\alpha - q_\alpha^* \left[\partial_t \delta q_\alpha + \frac{\partial X_{\alpha\beta}}{\partial q_\gamma} \delta q_\gamma \partial_x q_\beta + X_{\alpha\beta} \partial_x \delta q_\beta + \frac{\partial F_\alpha}{\partial q_\gamma} \delta q_\gamma - \delta f_\alpha \right] dV dt \quad (25)$$

The next step is to make δJ independent from δq , for this reason it is necessary to move all the derivatives applied to δq_α to the Lagrange multiplier q_α^* . This is done by using integration by parts:

$$\begin{aligned} \delta J &= \iiint q_\alpha^* \delta f_\alpha dV dt \\ &- \iiint \delta q_\alpha \left[\frac{\partial g}{\partial q_\alpha} - \partial_t q_\alpha^* + q_\gamma^* \frac{\partial X_{\gamma\beta}}{\partial q_\alpha} \partial_x q_\beta - \partial_x q_\beta^* X_{\beta\alpha} - q_\beta^* \partial_x X_{\beta\alpha} + q_\gamma^* \frac{\partial F_\gamma}{\partial q_\alpha} \right] dV dt \\ &- \left[\int q_\alpha^* \delta q_\alpha dV \right]_{t_0}^T \\ &- \left[\int q_\beta^* X_{\beta\alpha} \delta q_\alpha dt \right]_{L_0}^{L_x}. \end{aligned} \quad (26)$$

Equation 26 was split in four lines, to evidence some important terms. On the first line it is possible to see the dependency of J on f . From the second line it is possible to derive the adjoint equations, in fact to remove the dependency of δJ on δq it is necessary to equate the expression in the square brackets to zero, this gives the adjoint equations. The third and fourth line show, respectively, show the dependency of δJ on initial and boundary conditions. This terms have to be set to zero as well, and by doing so the initial and boundary conditions of the adjoint problem can be found, this will be discussed below.

Finally, the adjoint equations can be written:

$$\partial_t q_\alpha^* = q_\gamma^* \frac{\partial X_{\gamma\beta}}{\partial q_\alpha} \partial_x q_\beta - \partial_x q_\beta^* X_{\beta\alpha} - q_\beta^* \partial_x X_{\beta\alpha} + q_\gamma^* \frac{\partial F_\gamma}{\partial q_\alpha} + \frac{\partial g}{\partial q_\alpha}. \quad (27)$$

Notice that the equations are linear in \mathbf{q}^* . The explicit form of the equations is reported in [14] [17]. In the end the change of the objective function is given by

$$\delta J = \iiint \mathbf{q}^{*\top} \delta \mathbf{f} dV dt, \quad (28)$$

which can be seen as the gradient, or sensitivity, of the functional with respect to the control function \mathbf{f} .

An extension of these equations for the case of reactive flows can be found in [16]. The adjoint formulation for the Navier-Stokes equations employed in CuNSF code can be found in [14] [28].

3.2.1 Initial conditions

For the well-posedness of the adjoint system it is necessary that adjoint state is defined at the end of the considered time span and the system is integrated backwards in time [7]. This can be seen by imposing that the initial condition term in equation 26 to be zero.

$$-\left[\int \mathbf{q}^{*\top} \delta \mathbf{q} dV\right]_T + \left[\int \mathbf{q}^{*\top} \delta \mathbf{q} dV\right]_{t_0} = 0. \quad (29)$$

The right term vanishes as the state variables are set by the initial conditions of the direct system and therefore the variation must be zero. In the left term $\delta \mathbf{q}$ is arbitrary, and therefore it's necessary to impose that $\mathbf{q}^*(\mathbf{x}, T)$ is zero. Thus the temporal condition of the adjoint system is given at final time.

3.2.2 Boundary conditions

The form of the boundary conditions for the adjoint system is determined by the boundary conditions of the direct problem. In this work only one case will be considered and used, which is the non-reflecting boundary condition. For a detailed discussion about the general procedure for the derivation of boundary conditions for the adjoint system see [8] [7].

To derive the characteristic form it is necessary to rewrite the adjoint system 27 considering only the hyperbolic part, and therefore dropping all the other terms. The resulting equation can be written in the following form:

$$\partial_t \mathbf{q}^* + \mathbf{X}^*(\mathbf{q}) \partial_x \mathbf{q}^* = 0, \quad (30)$$

where the operator \mathbf{X}^* is

$$\mathbf{X}^* = \begin{bmatrix} u & 1/\rho & 0 \\ c^2 \rho & u & 0 \\ 0 & 0 & u \end{bmatrix}. \quad (31)$$

By doing an eigen-decomposition of the operator it is easy to find the eigenvalue matrix $\mathbf{\Lambda}$ and, respectively, the left and right eigenvectors matrices, \mathbf{L} and \mathbf{R} . The relation $\mathbf{X}^* = \mathbf{R}\mathbf{\Lambda}\mathbf{L}$ must be satisfied.

$$\begin{aligned} \mathbf{\Lambda} &= \begin{bmatrix} u+c & 0 & 0 \\ 0 & u-c & 0 \\ 0 & 0 & u \end{bmatrix} \\ \mathbf{R} &= \begin{bmatrix} 1/(\rho c) & -1/(\rho c) & 0 \\ 1 & 1 & 0 \\ 0 & 0 & 1 \end{bmatrix} \\ \mathbf{L} &= \begin{bmatrix} \rho c/2 & 1/2 & 0 \\ -\rho c/2 & 1/2 & 0 \\ 0 & 0 & 1 \end{bmatrix}. \end{aligned} \quad (32)$$

The waves are found by projecting the state variables vector onto the characteristics of the system

$$\begin{bmatrix} X^{*+} \\ X^{*-} \\ X^{*s} \end{bmatrix} = \mathbf{\Lambda}\mathbf{L}\mathbf{q}^* = \begin{bmatrix} (u+c) \left(\frac{c\rho}{2} \partial_x p^* + \frac{1}{2} \partial_x u^* \right) \\ (u-c) \left(-\frac{c\rho}{2} \partial_x p^* + \frac{1}{2} \partial_x u^* \right) \\ u \partial_x s^* \end{bmatrix}. \quad (33)$$

In the adjoint case the characteristic waves move in the opposite direction then from the direct case, that's because the adjoint system is integrated backwards in time. To impose the non-reflective condition on the boundary it's necessary to set the in-going waves to zero, just like in the direct case.

3.3. Objective function

The objective function is the fundamental piece of the data assimilation framework as it is the strictly connected to the forcing term of the adjoint equations. To derive the forcing adjoint term the general form of the functional to be minimized that it's going to be used in this work will be presented.

$$\begin{aligned} J &= \frac{1}{2} \int_{\Omega} \int_{t_0}^T (\psi - \psi_{exp})^2 \sigma_x(\mathbf{x}) \sigma_t(t) dV dt \\ &\approx \frac{1}{2} \sum_V \sum_{t_0}^T (\psi - \psi_{exp})^2 \sigma_x(\mathbf{x}) \sigma_t(t) \Delta x \Delta y \Delta z \Delta t \end{aligned} \quad (34)$$

the functional is evaluated using a discretized form. The variable ψ denotes a generic observable of the flow (e.g., pressure, temperature, velocity), ψ_{exp} corresponds to the target value of the observable, that is the desired value given by an experimental measurement. The numerical simulation is adapted towards that value. If measurements for multiple quantities are considered, the corresponding functions are summed.

The spatial function $\sigma_x(\mathbf{x})$ defines the observation region, that is the region of the domain in which the functional J is evaluated. The value of $\sigma_x(\mathbf{x})$ is one on the observation domain and zero outside of it. For the spatial case it is also necessary that $\sigma_x(\mathbf{x})$ is smooth, as the discontinuity could cause discontinuous excitations in the adjoint system, the regularization procedure is done using Gaussian smoothing. The time function $\sigma_t(t)$ indicates the time span of the observation, similarly to $\sigma_x(\mathbf{x})$ it is one in the observation time and zero outside of it. For this function smoothing is not needed.

The general form of the adjoint forcing term for our purposes is:

$$\frac{\partial g}{\partial \mathbf{q}} = (\psi - \psi_{exp}) \nabla_{\mathbf{q}} \psi \sigma_x(\mathbf{x}) \sigma_t(t). \quad (35)$$

3.4. Data assimilation framework

The adjoint formalism will be used to compute efficiently the gradient of the objective function. Adoint techniques are, in fact, particularly effective at computing high dimensional gradients, which is exactly what it is needed for this type of data assimilation. As it was proved in 3.2 the change of the objective function δJ and the change of the forcing term δf are related by equations 28. It is possible to find:

$$\nabla_{\mathbf{f}} J = \mathbf{q}^*, \quad (36)$$

where here the term $\nabla_{\mathbf{f}} J$ is to be understood as a Fréchet derivative [1]. Therefore the gradient of the objective function J with respect to the forcing term \mathbf{f} is the solution of the adjoint equations. It provides an optimal direction to minimize the objective.

The gradient is determined on all the computational domain, however, to maintain the physicality of the solution in the observation region the forcing term is adapted only outside of the measurement region. Thus a spacetime weight $\theta = \theta_x(\mathbf{x})\theta_t(t)$, similar to the σ weight, is applied on the gradient, this weight defines the region of adaptivity of \mathbf{f} .

The gradient of the objective is used to perform a steepest descent algorithm

$$\mathbf{f}^{n+1} = \mathbf{f}^n - \alpha \nabla J(\mathbf{q}^n), \quad (37)$$

the actual forcing is updated iteratively using the adjoint solution. The parameter α is the step width, which must be carefully chosen to guarantee a good convergence behavior.

This optimization procedure can be accelerated and made more accurate by implementing *line search* methods and *non linear conjugate gradient* techniques. The former are a family of methods that iteratively change α in an optimal way, to ensure a big step width and therefore a fast convergence rate [23]. The latter is a family of techniques that generalizes the *conjugate gradient* method to non linear optimization problems [10] [23]. It improves the steepest descent method, which presents bad convergence properties for ill-conditioned objective functions, by selecting a direction of descent that depends not only on the gradient computed in the current iteration but also the previously used gradients and directions. For this work these improvements were not necessary, as the simple gradient descent method was enough to have good convergence properties, and therefore more sophisticated optimization methods were not used.

3.4.1 Iterative framework

Now that the main concepts of the data assimilation procedure have been laid down, it is possible to construct an iterative procedure to find the optimal \mathbf{f} that generates the flow that minimizes J .

Starting from an initial condition, the Navier-Stokes equations are solved forward in time. Afterwards the objective function is computed and the adjoint equations are solved backwards in time, using $\frac{\partial g}{\partial \mathbf{q}}$ as the adjoint forcing. From the adjoint solution the gradient of the objective is obtained and the forcing term \mathbf{f}^n is adapted, and then the procedure starts again with a new forcing term for the Navier-Stokes equations. The loop stops when a convergence criteria is met, e.g., number of loops, value of J and change of the value of J .

It's important to state that the detection of a global minimum is not ensured and that the framework minimizes towards a local minima. Furthermore, depending on the individual setup, the solution may not be unique.

Algorithm 1 Data assimilation procedure

```

Initial guess  $\mathbf{f}^0$ 
while  $J > \epsilon$  or  $i < N$  do
  Solve Navier-Stokes equations  $N(\mathbf{q}, \mathbf{f}^n)$  (direct solution).
  Compute  $J$ .
  Solve the adjoint Navier-Stokes equations  $N^*(\mathbf{q}, \mathbf{q}^*, \mathbf{f}^n)$ .
  Compute the gradient  $\nabla_{\mathbf{f}} J(\mathbf{q}, \mathbf{q}^*, \mathbf{f}^n)$ .
  Update  $\mathbf{f}^{n+1} = \mathbf{f}^n - \alpha \nabla_{\mathbf{f}} J(\mathbf{q}, \mathbf{q}^*, \mathbf{f}^n)$ .
   $i = i + 1$ 
end while

```

3.5. Data assimilation of Initial Conditions

Data assimilation is not necessarily constrained to adaptation of the forcing term, it can also be possible to assimilate initial and boundary conditions [9]. In this work the initial conditions of a compressible starting jet will be assimilated, therefore it is necessary to develop the data assimilation of initial conditions procedure. For a more detailed discussion of data assimilation of boundary conditions see [14] [1].

In general, the initial condition of a particular flow can be rewritten as a generic function of space

$$\mathbf{q}(\mathbf{x}, t = 0) = \mathbf{s}(\mathbf{x}). \quad (38)$$

In the linearized case one can write $\delta \mathbf{q}(\mathbf{x}, t = 0)$. This last term can be added to the Lagrangian formulation 26 with a separate Lagrangian multiplier \mathbf{s}^* .

$$\delta J = \dots - \mathbf{s}^{*\top} (\delta \mathbf{q}(\mathbf{x}, t = 0) - \delta \mathbf{s}(\mathbf{x})). \quad (39)$$

The integrals are omitted for readability. The variation $\delta \mathbf{q}(\mathbf{x}, t = 0)$ corresponds to the temporal term in 26. The combination of the variations $\delta \mathbf{q}(\mathbf{x}, t = 0)$ leads to

$$\delta \mathbf{q}^\top(\mathbf{x}, t = 0) (\mathbf{q}^*(\mathbf{x}, t = 0) - \mathbf{s}^*(\mathbf{x})) = 0. \quad (40)$$

In this case the term in the parenthesis must be zero, as the variation of the initial condition must be assimilated and therefore it can be different from zero. The gradient follows from the product of \mathbf{s}^\top with $\delta \mathbf{s}(\mathbf{x})$ in 39 and results in:

$$\nabla_{\mathbf{s}} J = \mathbf{s}^*(\mathbf{x}) = \mathbf{q}^*(\mathbf{x}, t = 0). \quad (41)$$

Therefore the initial condition must be adapted using the last timestep of the adjoint solution, as it is solved backwards in time.

3.6. Verification case

This example is used to verify the developed data assimilation framework and to showcase its effectiveness. This case was already performed in [29] [14] [19], here it will be carried out using the newly developed CuNSF code, and the results will be replicated.

3.6.1 Setup

In this example the objective is to assimilate the sound source of a simple compressible acoustic setup. The setup consists of a point wise speaker surrounded by eight microphones, everything is set on a common plane, as all the simulations will be two dimensional. The numerical simulation will be done with the fully compressible Navier-Stokes equations. The speaker will emit an harmonic signal at 1kHz. The observation region is defined by the microphones and therefore the objective function is formulated in terms of pressure measurements at the microphone locations. Therefore the adjoint forcing term is given by the difference of the assimilated p and

the measured data p_{exp} . The special weight σ_x is defined as sharp Gaussian distributions in the location of the microphones, σ_t is one for all time. The initial guess is $\mathbf{f}^0 = 0$.

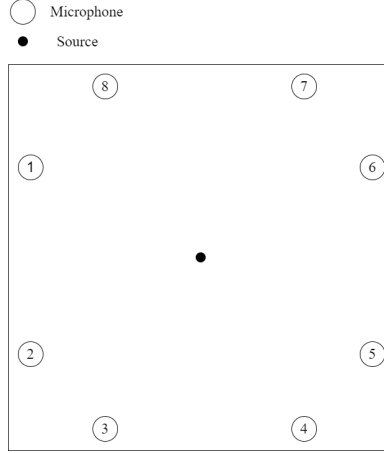


Figure 2: Numerical experiment setup for the acoustic case.

The computational domain, as can be seen from 2, is a 1×1 square resolved by a 128×128 grid. The CFL number is 0.9. All the boundaries are non-reflective.

3.6.2 Source identification

In the context of the mentioned setup the first adjoint solution is sufficient for the identification of the position and frequency content of the sound source, but insufficient for the amplitude information.

For the position identification it is possible to use the point wise summation of the absolute pressure adjoint sensitivities over all the computed time steps:

$$\hat{p} = \sum_{t=0}^T |p^*|, \quad (42)$$

the positions of maximum impact on the loss function are identified by the maximums of the function \hat{p} . These are the most likely source positions.

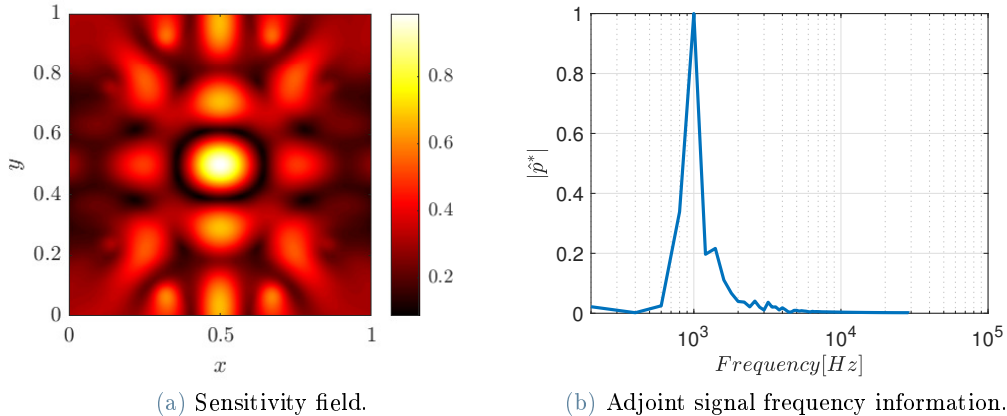


Figure 3

In figure 3 the resulting pressure sensitivity field \hat{p} is shown. It is possible to see a clear global maximum in the middle of the domain, that is the most likely point of sound generation. The other local maxima are caused by interference effects in the adjoint pressure. A unique solution cannot be identified.

The frequency information can be extracted from the first adjoint solution as well. This is because it contains

an update of the initial forcing $\mathbf{f}^0 = 0$. A frequency analysis of the adjoint signal p^* shows that the harmonic reference signal is recovered, see figure 3.

3.6.3 Source assimilation

A full data assimilation is then done on the partial acoustic measurement provided by the microphones. The algorithm successfully converged, see figure 4, and identified a possible solution of the measured flow. From the assimilated signal the amplitude information can be recovered, giving the possibility to completely identify the acoustic source.

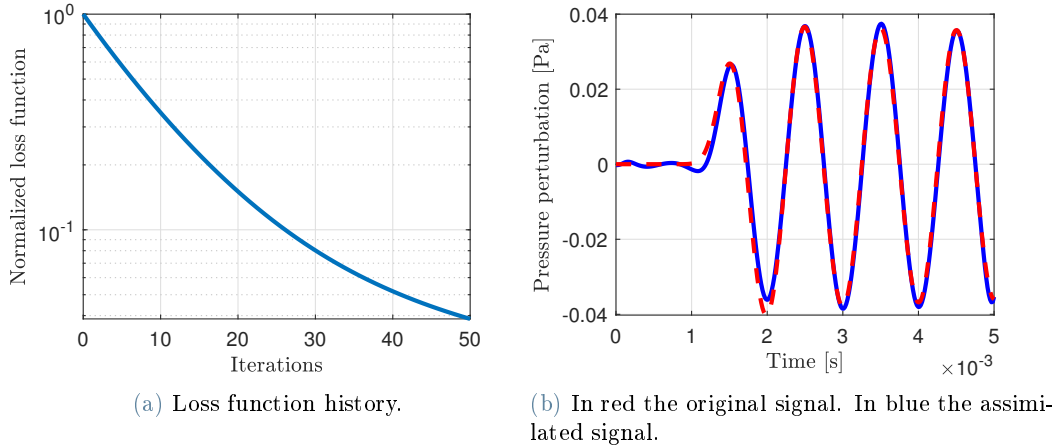


Figure 4

The framework is therefore able to assimilate sources from (synthetic) experimental measurements in the context of the previously defined acoustic setup governed by the Navier-Stokes equations. This not only serves as a validation of the framework and of the CuNSF code, but it is also a demonstration of one of the vast possible scenarios in which the adjoint based data assimilation can be used. In particular, the adjoint based source reconstruction can be of interest in the context of sound field synthesis.

4. Data assimilation of Kovasznay modes

In this chapter the data assimilation of the Kovasznay modes [13] will be presented. These modes are a result of the linearization of the fully compressible Navier-Stokes equations, and they give rise to a set of wave-like solutions that are, in a first order approximation, completely independent of each other.

The objective of this chapter is to test the observational capabilities of the derived assimilation framework and see if it is able to observe second-order effects of first-order approximate solutions. This will be done by finding the flow that better approximates the single mode solution, (i.e., pressure acoustic wave), and see the reconstructed flow in the other variables (e.g., vorticity field and entropy field). This observability analysis is of particular interest as it can be used as a benchmark for all the other possible compressible flows.

4.1. Kovasznay modes

Kovasznay [13] theoretically investigated the response of a hot-wire under exposure of a compressible flow. The objective was to see what information the hot-wire was able to retain from the measured flow of interest. To do so he derived a set of linear independent equations. Here, a short description of the method will be presented. Kovasznay performed a linear expansion of the Navier-Stokes equations for a perfect gas and for small perturbations around a base state. After some manipulations the resulting set of equations was found:

$$\frac{\partial \omega}{\partial t} - \nu \nabla^2 \omega = 0 \quad (43a)$$

$$\frac{\partial s}{\partial t} - \frac{4\nu}{3} \nabla^2 s = 0 \quad (43b)$$

$$\frac{1}{c^2} \frac{\partial^2 p}{\partial t^2} - \nabla^2 p - \frac{4\gamma\nu}{3c^2} \frac{\partial \nabla^2 p}{\partial t} = 0. \quad (43c)$$

The solutions of these equations yield the three fundamental modes of compressible turbulent flows. From the results, it is possible to see that two modes obey the heat equation, but with different diffusion coefficients, and the third mode obeys the wave equation with an absorption term. The vortical mode corresponds to velocity perturbations, the acoustic mode corresponds to perturbations of pressure, velocity and density and propagate as sound waves, the entropy mode corresponds to perturbation of temperature, density or pressure. For each of these equations it is possible to assume plane wave solutions:

$$\boldsymbol{\omega} = \boldsymbol{\omega}_0 e^{ik(\mathbf{n}\cdot\vec{\xi}) - t/t_1} \quad (44a)$$

$$p = p_0 e^{ik(\mathbf{n}\cdot\vec{\xi}) - Ct} \quad (44b)$$

$$s = s_0 e^{ik(\mathbf{n}\cdot\vec{\xi}) - t/t_3}. \quad (44c)$$

Where $t_1 = 1/\nu k^2$ is the vorticity decay time, $C = c\sqrt{1 - \left(\frac{2k\gamma\nu}{3c}\right)^2} - i\left(\frac{2k\gamma\nu}{3}\right)$ gives the propagating velocity and decay time of the pressure wave, and $t_3 = 3/4\nu k^2$ is the entropy decay time.

In a more general case, however, these modes can have higher order interactions between themselves. If second order terms are small compared to first order terms, then these can be added to the mode equations as source terms:

$$\frac{\partial \boldsymbol{\omega}}{\partial t} - \nu \nabla^2 \boldsymbol{\omega} = \boldsymbol{\Omega}(\boldsymbol{\omega}, p, s) \quad (45)$$

$$\frac{\partial s}{\partial t} - \frac{4\nu}{3} \nabla^2 s = S(\boldsymbol{\omega}, p, s) \quad (46)$$

$$\frac{1}{c^2} \frac{\partial^2 p}{\partial t^2} - \nabla^2 p - \frac{4\gamma\nu}{3c^2} \frac{\partial \nabla^2 p}{\partial t} = P(\boldsymbol{\omega}, p, s). \quad (47)$$

An observation analysis will be done, trying to extrapolate these source terms by assimilating the modes singularly. The goal of the chapter is understanding how much can be inferred about unknown variables, given perfect information on a single mode using data assimilation.

4.2. Results

In this section the results of the assimilation for the modes will be presented, the reconstruction of the flow in the middle time steps will be evaluated, and the capacity for the assimilation framework to infer information about unknown modes from the reconstructed mode will also be assessed.

For the assimilation, two dimensional plane-wave solutions were constructed. The wave-number is the same for all the modes $k = 6\pi$ and the computational domain is the same as the one described in Section 2.3.

The assimilation setup used is the same as the one that is going to be used for the data assimilation of the jet, as this observational results will be used as benchmark for the assimilation of more general and complex flows, like the starting jet. Only two snapshots of the modes will be given as input to the algorithm and the reconstruction in the time span in between the two snapshots will be evaluated. The time jump between the two snapshots is going to be of the same order of magnitude of the jet case in section 5.2, as this part of the work is preparatory to the jet case.

4.2.1 Pressure mode assimilation

For the pressure mode case, it is possible by looking at figure 5 to see that the reconstruction of the pressure mode in the middle time step is successful, as the assimilated flow matches very well with the real flow. The framework was also able to reconstruct part of the entropy mode successfully, given the information on the pressure mode only. However the vorticity mode was not reconstructed by the data assimilation. It is important to note that this does not mean that the assimilation framework did not find a possible velocity flow, to be more precise, from the knowledge of the pressure mode it is possible to find a velocity flow that is irrotational, as the information about a possible potential flow is not found in the vorticity mode, but in the pressure mode. The velocity field u that was found has the same wave-number and same phase of the pressure field that was assimilated, this confirms the fact that is the pressure mode equation that drives the potential-dependent component of the velocity field. In general, it is expected that the knowledge on a single scalar field is not enough to reconstruct in a satisfying manner an entire vector field.

The amplitude of the reconstructed entropy mode is also important to look at. In this case the amplitude of the reconstructed mode is of the same order of magnitude of the assimilated signal, this implies a strong correlation between these two modes.

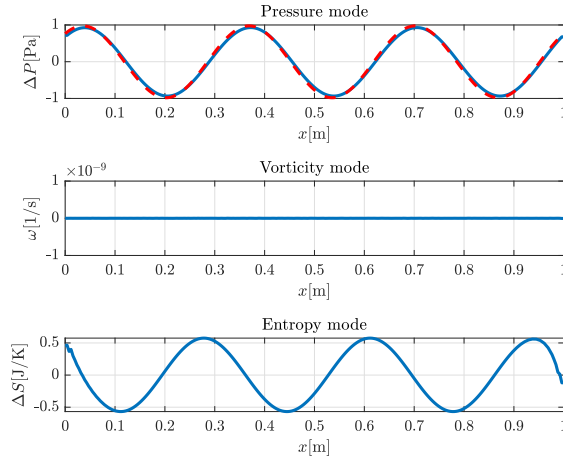


Figure 5: Results of the assimilation of the pressure mode in the middle time step. In red the observed mode, in blue the result of the assimilation

4.2.2 Vorticity mode assimilation

Also for the vorticity mode case the reconstruction of the middle time step is successful, as it is possible to see from figure 6. In this case the method was also able to find a contribution of the vorticity mode into the pressure and entropy mode. This, however, leads to the reconstruction of an aliasing of the original signal. This fact is not surprising, as the modes are independent of each other, at least in the first order approximation case, and therefore there can be multiple possible reconstruction. This makes the problem ill-posed, and data assimilation can find a possible solution that might not be correct. In this case the assimilation framework found an incorrect, but physically possible, reconstruction of the pressure and entropy mode from the knowledge of the vorticity information. This sort of phenomena are frequent in variational data assimilation, and are generally caused by a pronounced ill-posedness of the problem in hand. It is also important to mention that, just like in the previous section 4.2.1, an effect on the velocity field u is found, and it has the same properties of the reconstructed pressure mode.

By looking closely at the reconstructed modes it is possible to see how the peaks of the reconstructed signals correspond to the peak regions of the assimilated signal and its derivatives. This implies an important correlation and sensitivity of the pressure and entropy perturbation with respect to velocity perturbation and its gradients.

The amplitudes of the entropy and pressure however are very small, which implies that the capacity of reconstruction of the method is not particularly strong.

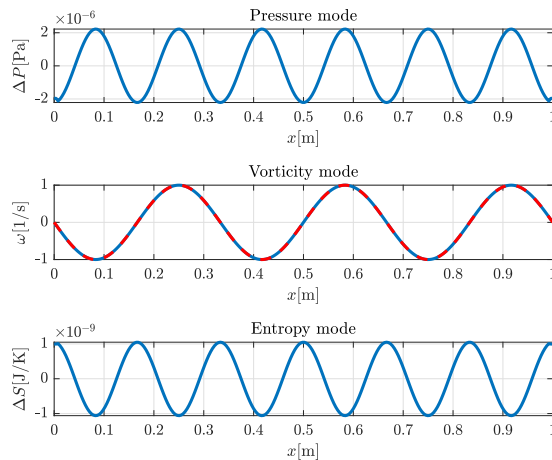


Figure 6: Results of the assimilation of the vorticity mode in the middle time step. In red the observed mode, in blue the result of the assimilation

4.2.3 Entropy mode assimilation

Similarly to the above cases, it is possible to see from figure 7 that the assimilation of the entropy mode in the middle time step is successful. The reconstruction of the vorticity mode, however, is not successful, just like in pressure case. The pressure mode reconstruction is also not completely successful, as the pressure mode found has double the wave number of the assimilated wave.

From the previous analysis it is possible to say that the entropy mode is the mode with the least amount of information of all the Kovaszny modes.

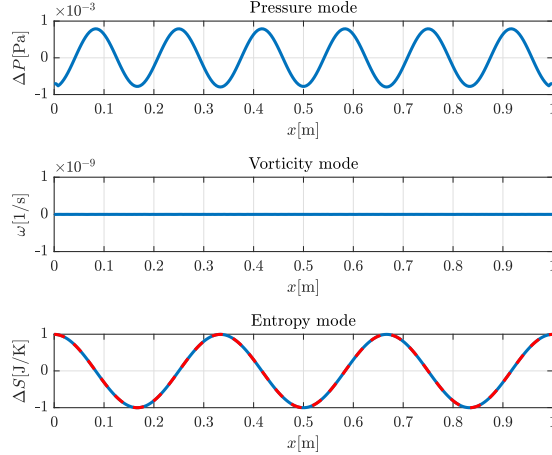


Figure 7: Results of the assimilation of the entropy mode in the middle time step. In red the observed mode, in blue the result of the assimilation

5. Data assimilation of the compressible starting jet

In this section the data assimilation of a compressible starting jet will be presented. This data assimilation is of particular importance, as it will be used as the first step towards a full data driven DNS of a compressible flow from limited real-world data. The objective of this section is to test the observability capabilities of the previously derived data assimilation framework for the compressible starting jet. Given a limited amount of information about the flow, the objective is to see what is possible to reconstruct. The analysis will be done systematically, using a single given field of the flow (e.g, pressure, temperature, density etc...) at two different times and the flow will be reconstructed in the middle time steps. The L_2 norms between ground truth and the assimilated flow will be compared, to see how much of a certain unknown field it is possible to reconstruct from another known field. This study will be performed in light of the assimilation of the Kovaszny modes study that was done in section 4, as it will be of great importance to understand the results.

The systematic study will not only be performed with respect to the amount of information that will be given to the algorithm, but also with respect to the time distance between each snapshot. It is expected that the reconstruction capabilities of the middle time steps of the data assimilation framework worsens as the time distance between the two given snapshots increases, however it is not possible to know a-priori how much does the error increase with respect to the time. In this section the amount of error growth with respect to the time steps used is going to be assessed.

5.1. Simulation setup

The data assimilation will be done on synthetic data generated by a DNS of a compressible starting jet. For the current case the domain and boundaries that will be used are the ones described in 2.3. The jet's mass supply is considered as infinite. The Reynolds number is set to $Re = UD/\nu = 5000$, where U is the characteristic velocity of the jet, D is the diameter of the inlet and ν is the kinematic viscosity. The Mach number is set to $M_\infty = U/c = 0.8$ and the pressure jump between the reservoir and the open chamber is selected as $p_r/p_\infty = 1.5$. According to [5] a grid of 512×512 is good enough to capture the Kolmogorov small scales in this particular jet case. The CFL number selected is $CFL = 0.8$, the reason why it's selected as big as this is because we want to maximize the time jump between each time step. The time step found is, therefore, $\Delta t = 4.5 \times 10^{-6}$ seconds.

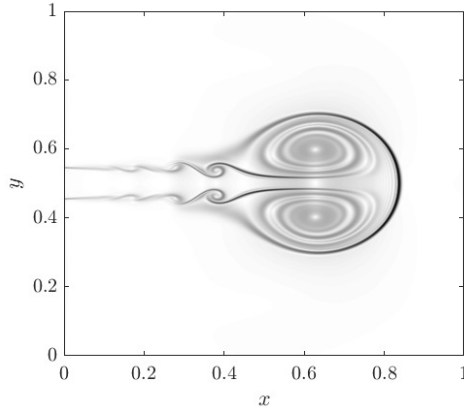


Figure 8: Numerical schlieren ($||\nabla\rho||$) of the jet at time $t^* = 27.86$.

5.2. Data assimilation setup

The assimilation setup is analogous to the case developed in section 4. Two snapshots of the flow are selected and are used as synthetic experimental data to make the data assimilation happen. The goal will be to assess the precision of the assimilation in the middle time steps and the capability of the data assimilation framework to reconstruct the jet flow taken into consideration. In the first case only a single time step jump will be considered, then the time steps will be increased to nine and seventeen. The selection of such a small time gap between the two synthetic measurements is justified by the actual laboratory instruments present in the research group's laboratories. In fact, the group owns a high-speed camera that is able to take images at the order of 10^{-6} seconds. The goal is to make the synthetic experiment similar to the real world experiments that will be done in the future at the research group.

The systematic study will not only be done using time steps, but also by doing the data assimilation on partial data of the flow. The choice of chosen data is motivated by possible experimental setups for flow visualization and measurement. In this work the following cases will be presented: assimilation of pressure (microphone), assimilation of velocity field u (hotwire), assimilation of velocity field v (hotwire), assimilation of velocity vector field $(u, v)^T$ (Particle Image Velocimetry), assimilation of temperature field (thermal camera), assimilation of density field (shadowgraph) and full state variables assimilation $(p, u, v, s)^T$ for reference. In this work the schlieren assimilation will not be considered. The errors are defined as:

$$err = \frac{||q - q_{gt}||_{L_2}}{||q_{gt} - q_0||_{L_2}}, \quad (48)$$

where q is the solution found by the data assimilation, q_{gt} is the correct field (or ground truth) and q_0 is ambient field. This error measures how close the assimilated field is to the real one with respect to the perturbation of the real flow with respect to the ambient condition. The L_2 norm is defined only on the spacial domain, and it's computed in the time step that is placed in the middle of the snapshots used for the data assimilation.

5.3. Results

5.3.1 Full case

The full case is here presented as reference. In this case all the state variables are used for the assimilation, therefore no reconstruction is evaluated. Looking at figure 9 it's clear to see that all the flow in the middle time step is assimilated successfully. The best performing fit is on the thermodynamic variables, with temperature being the best and density being the worst. The trend of all the thermodynamic variables is very similar between each other. Entropy is the most different, as it behaves similarly to an exponential.

The velocity variables have a worse performing fit with respect to the thermodynamic variables. The vertical velocity v is the worse performing approximation of all the fields. The horizontal velocity u and the vorticity field ω behave exactly the same, this indicates that they are highly correlated between each other. This is expected as in the case of a jet u is the dominant component of the velocity vector, and the vorticity is mostly generated by the horizontal component of velocity. Both u and ω almost behave like exponentials.

The full case is, out of all the cases, the best performing. This is expected, as full knowledge of the flow is fed to the data assimilation algorithm, and finding a good fit for the data knowing everything about the flow is easier.

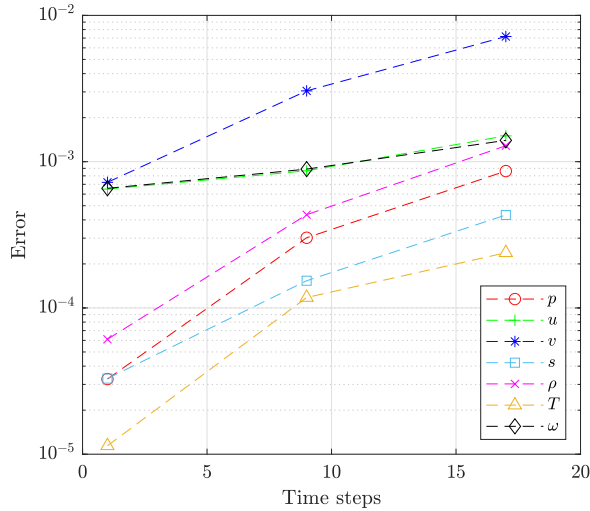


Figure 9: Error trends of the fields in the middle time step with respect to the time steps jump in between the snapshots used for the data assimilation in the full case.

5.3.2 Pressure case

Here the pressure case is presented. This case is considered as an observability benchmark for pressure experimental measurements, mostly done by microphones. Differently from the previous case, also the reconstruction capabilities of the assimilation will be assessed here, as only the pressure measurements were observed for this data assimilation.

From figure 10 it is possible to see that the middle step assimilation of the pressure measurement was successful,

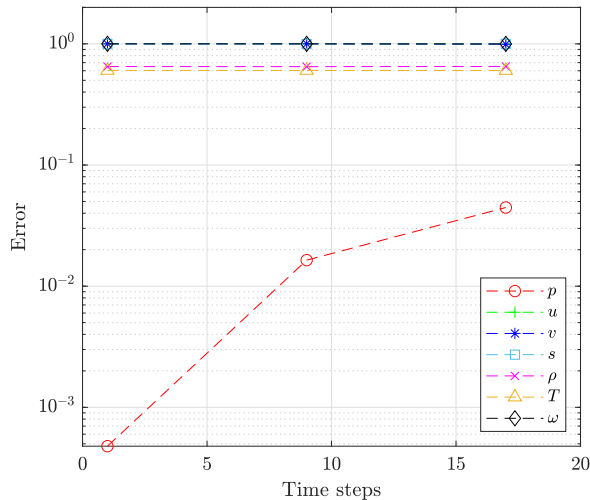


Figure 10: Error behavior of the fields in the middle time steps with respect to the time steps jump in between the snapshots used for the data assimilation in the pressure case.

as the error is small for all the analyzed cases. The pressure error trend of this case is similar to the trends in figure 9 in the full case. However the precision of the assimilation in the full case is higher than the pressure only case. Looking at the trends of the other thermodynamic variables it is possible to see how the error norm of the density and temperature are smaller than one. This means that part of the field was reconstructed successfully. The error doesn't change in any meaningful way by increasing the time steps, this is because the error difference in the pressure assimilation is small with respect to the temperature and density error norms, and it doesn't impact the error norms in a significant way. The error norm of temperature and density are, respectively 0.60 and 0.65. The reconstruction is partial because the knowledge on the entropy is absent, and therefore the reconstruction of thermodynamic variables is partial, and it's due to the pressure information only. This is not enough because in the case of a perfect gas, two thermodynamic variables must be known to have a complete thermodynamic description of the flow. This effect can be seen well by looking at figure 11. Looking

at the reconstructed temperature field in figure 11b and comparing to the assimilated pressure field 11a it's possible to see how the two flow configurations are very similar with one another, this is because we only see the pressure field part that composes the temperature field. When looking at the localized error, computed as $\frac{|q-q_e|}{\max(q_e)-\min(q_e)}$, in figure 11c it is possible to see that the error configuration is extremely similar to the entropy field configuration. This is expected since in the reconstructed temperature field the entropy information is completely absent and it must show in the error.

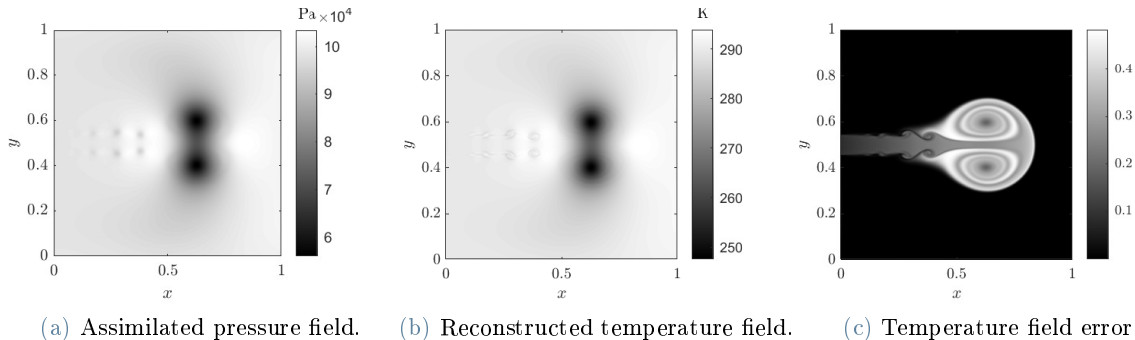


Figure 11

Looking at the error norms of the velocity components and vorticity fields it is possible to see that the reconstruction of velocity variables was not successful. In fact the error norms for u , v and ω are all approximately one. This indicates that no significant reconstruction can be detected, at least in an integral sense. However, by looking closely at the velocity fields it is possible to get more information about the reconstruction done out of the pressure field of the jet. By taking into consideration figure 12, it is possible to see that the velocity flow that is reconstructed by the data assimilation is a potential flow. In fact, by looking at, u and v one sees that the reconstructed flows are simply sinks located where the two-dimensional vortices of the jet are. The bigger the vortex the bigger the sink. Notoriously these flows are irrotational and therefore are potential flows. This effect is not a surprise, in fact this was predicted in the previous discussion on Kovasznay modes, when the pressure mode was assimilated in section 4.2.1. The reason why it is only possible to see potential velocity flows stems from the Navier-Stokes equations for the velocity components 1b. The only dependence of velocity on pressure inside of the equation is through a gradient, therefore the only possible contribution pressure can make, under the hypothesis of a continuous flow, must be irrotational. The reason why this effect is not detected in the error norm analysis is because the reconstructed flow is small in amplitude, and it cannot be seen properly using an integral norm.

For the entropy, something analogous happens, as it depends mostly on the temperature second derivative, as it can be seen from (1c), which looks similar to the pressure field. The image is not reported here for brevity. Differently from what happened with the Kovasznay case, the entropy assimilation was not very effective, especially when it comes to amplitudes. This is because of the nature of the flow. The main contributions in the jet flow are due to convective effects from the boundary conditions, this makes pressure-entropy interactions less dominant. The Kovasznay modes analyzed in section 4 are flows in a linear regime, whereas this case is highly nonlinear, and the observational effects might not always be comparable.

5.3.3 Velocity vector field $(u, v)^T$ case

The velocity vector field data assimilation is now presented. This case will be used as an observability benchmark for experimental PIV measurements.

The assimilation in the middle time step is successful as it can be seen from figure 13. Just like it is expected the full case is better performing when it comes to precision. Similarly to the full case the vertical velocity v is slightly less precise than the horizontal velocity. As a consequence of well assimilated velocity vector also the vorticity of the flow is well reconstructed.

The thermodynamic variables, however, are not well reconstructed. This is analogous to the pressure case in section 5.3.2, as the norms are not able to capture the amount of information that the assimilation framework is able to extract from the partial information. It can be seen, by looking at figure 14, that the reconstructed pressure field and the velocity divergence field have a very similar configuration, with inverted signs. This is because in the compressible Navier-Stokes equations the divergence of the velocity field works as a source term, with inverted sign in the pressure equation. However this effect is not big and complete enough to reconstruct in a satisfying manner the pressure field. This also affects the temperature and density field, which have config-

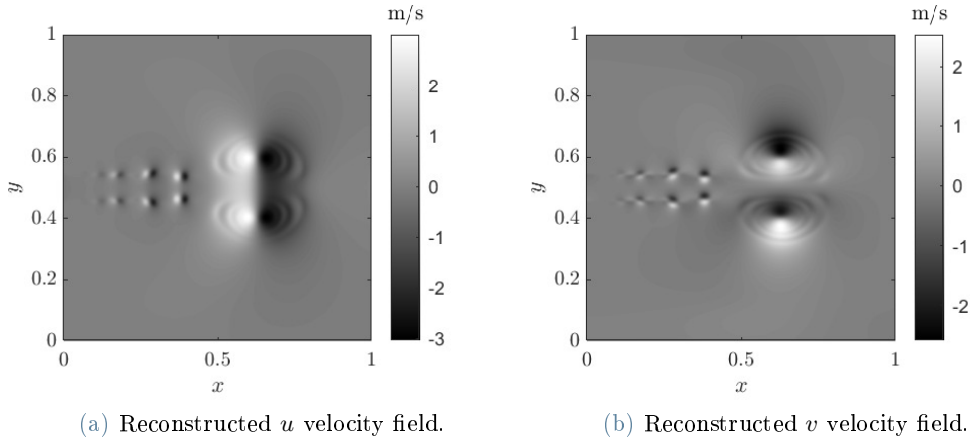


Figure 12

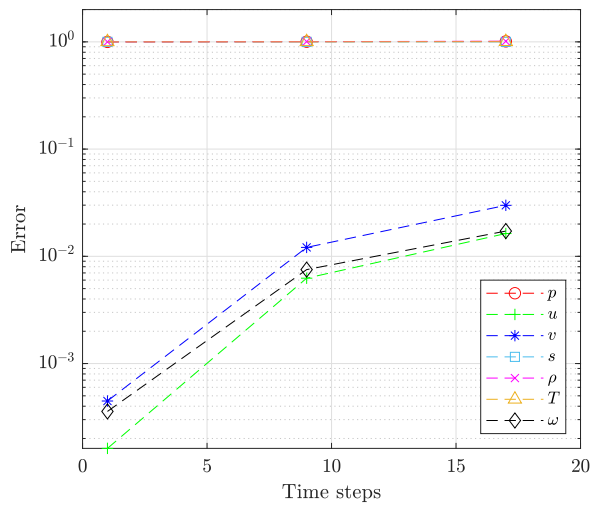


Figure 13: Error behavior of the fields in the middle time steps with respect to the time steps jump in between the snapshots used for the data assimilation in the velocity vector field case.

urations that are similar to the pressure field configuration. This same effect can be seen on the entropy field, because the viscous dissipation term in equation 1c is perfectly reconstructed. However this reconstruction doesn't have much of an effect in the global computation of the error norm.

This capability of reconstruction of thermodynamic variable from vorticity information was predicted by the Kovasznay modes analysis in section 4.2.2, and it was also predicted that its effect would be very small with respect to the values of the original vorticity mode.

5.3.4 Velocity field u and v case

Here the data assimilation of the single velocity fields u and v are presented. These two cases are presented together for brevity and because the results are similar to each other. These results will be used as observability benchmark for experimental hot wire measurements.

Looking at figure 15 it's possible to see that the assimilation in the middle time step is again successful. The precision on the assimilation is again higher for the u field then for the v field. It's also very interesting to see that for the u field assimilation case it is possible to reconstruct a very big part of the vorticity and a small part of the vertical velocity field. Another interesting fact is that by increasing the time step the reconstruction capabilities of the method increase. In fact $\omega = 0.32$ and $v = 1$ for the single time step case, and they decreases to $\omega = 0.27$ and $v = 0.96$ for the 17 time steps case. This reconstruction effect is small and it's mostly due to the velocity diffusion effects that can have effect when the time frame for the direct simulation increases. This effect however is not replicated with the assimilation of the v field.

The reconstruction capabilities of the data assimilation given the single velocity fields is very limited. The effects

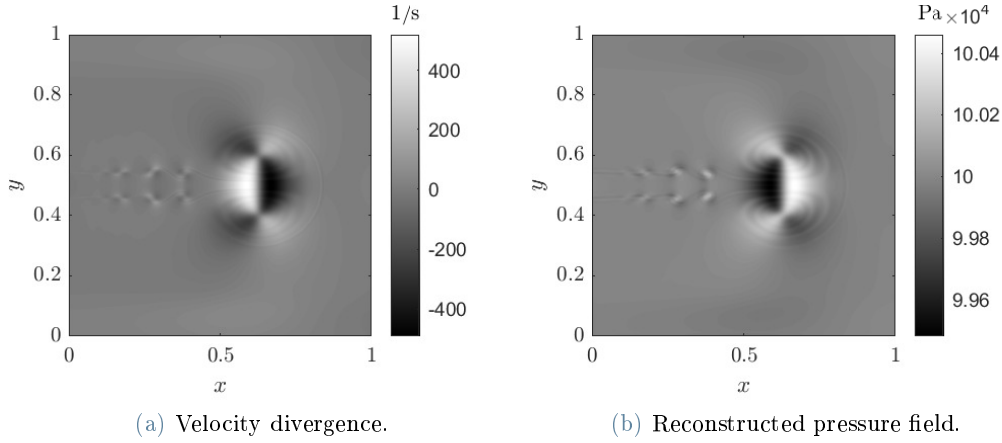


Figure 14

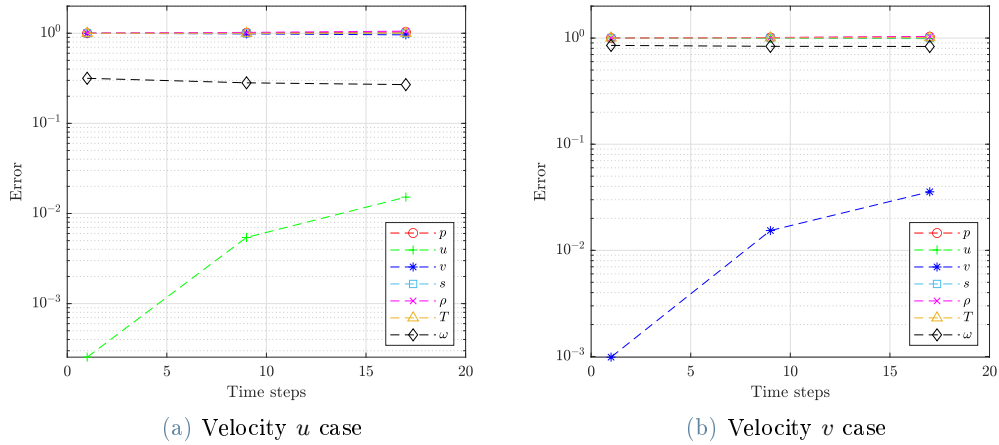


Figure 15: Error behavior of the fields in the middle time steps with respect to the time steps jump in between the snapshots used for the data assimilation of the velocity field u and v separately.

due to the interaction between pressure and velocity divergence is very weak and partial due to the fact that only one of the components of the velocity is known. This is also true with the viscous dissipation in the entropy equation. Because of incompleteness of the information the reconstruction of the fields is not satisfactory.

5.3.5 Temperature and density case

The data assimilation of the temperature and density fields are here presented. These two cases are reported together because of their similarity. The results will be used as observability benchmarks for temperature measurements done with a thermal camera and for optical measurements done with the shadowgraph technique. The data assimilation is successful in the middle time step for both cases, however for the 17 time steps case the precision becomes rather low, and the assimilated solution is somewhat inaccurate. This can be seen in figure 16.

The inaccuracy can be explained by the incapability of the framework to reconstruct information of the velocity field. The lack of this information makes impossible for the temperature and density field to be transported forward while time passes. This effect is remarked by the fact that the jet flow is an advection dominated flow, and this effect is especially important for thermodynamic variables like temperature, density and entropy.

Looking at the reconstruction of the thermodynamic variables something interesting happens. When doing the data assimilation on the temperature field, the error on the density field is bigger than without any assimilation at all. The reason for this can be seen in figure 17. The reconstructed field is correct for most of the domain, however a big error is generated in the middle of the two vortices, in which the pressure becomes very low. The reason of this error is due to the fact that the pressure information is not well reconstructed, and the method cannot see the big pressure jump in the high vorticity regions. Because of this big localized error, the integral norm becomes very large and the error defined by equation 48 is large. This however, doesn't mean that part

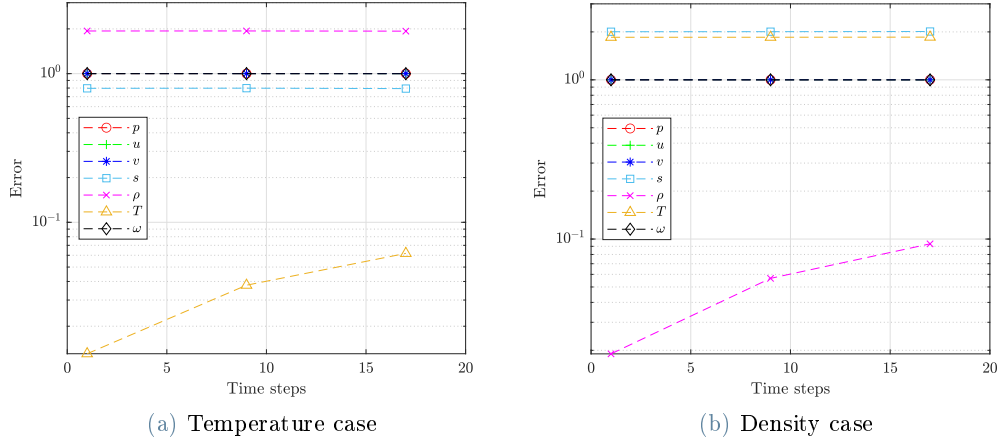


Figure 16: Error behavior of the fields in the middle time steps with respect to the time steps jump in between the snapshots used for the data assimilation of the temperature and density field.

of the field is not reconstructed. The same effect can be seen in the density assimilation case. When density is assimilated the integral error for the entropy and temperature fields increases. This phenomenon is analogous to the observability effect in the pressure case in section 5.3.2, thermodynamic variables depend on two state variables, knowing just one is not enough and the error one makes in the reconstruction depends completely on the unknown field.

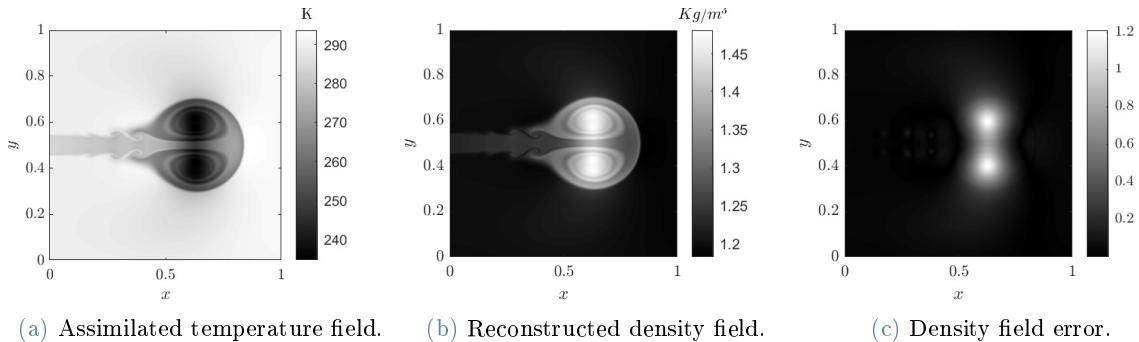


Figure 17

6. Conclusions

The observation analysis for the derived data assimilation was done to understand the reconstruction capabilities of the adjoint-based data assimilation procedure. First, the method was validated successfully on a simple acoustic case. The frequency content of the acoustic source was resolved, the position of the sound source was found and the amplitude of the signal was assessed correctly.

Second, the reconstruction capabilities of the data assimilation procedure on the Kovasznay modes was investigated. The analysis showed that the DA framework was able to reconstruct all the observed modes correctly in the middle time steps. The reconstruction capabilities with unknown fields was not completely satisfactory. From thermodynamic variables like pressure and entropy it is impossible to reconstruct a non potential velocity flow, that is, from the entropy and pressure modes it is impossible to reconstruct the vorticity mode. In general, this is expected, as velocity is a vector field, and thermodynamic variables are scalar fields. Reconstructing a vector field from a scalar field is not easy, as the latter has a lower dimension, and therefore less information with respect to the former. The reconstructed variables are in general with very low amplitudes with respect to the originally assimilated signal. This implies low reconstruction capabilities.

Finally, the observational analysis is repeated on the compressible starting jet in a systematic manner on various variables of experimental interest. The data assimilation was able to generate a flow that matched the ground truth in the middle time steps, but only for the variables that were being observed. The developed procedure

was not able to find the entirety of the unknown variables, just part of them. The reconstructed flows were directly linked with explicit and easily identifiable terms in the compressible Navier-Stokes equations. However the reconstruction capabilities were unsatisfactory in some cases.

The cause of this ineffectiveness is to be found in the fact that jets are flows in which the convective component is very strong with respect to all other effects. Assimilating the velocity field gives information on the convection field but does not give any information on the other fields that are being advected, not even on the boundary and initial conditions. This makes inferring other unknown variables very hard.

It was previously demonstrated that the pressure variable can be inferred from PIV measurements in compressible flows [18] [14]. In that case however the convection flow was considered as a base flow, and therefore the initial condition for both the direct solution of the data assimilation and of the ground truth was the same. This means that the initial condition was perfectly known, for each variable. This is not the case for the compressible starting jet here presented. Additionally, the time frame of the assimilation done in this work is much smaller than the previously cited one. This makes it impossible for the direct solution to transition from an unstable assimilated solution to a stable one. The space of stable solutions of the Navier-Stokes equations is a much smaller space than the unstable solutions space, especially for high Reynolds number flows. The requirement of being stable makes the work of finding the correct solution easier because it bounds the flow in a smaller solution space.

References

- [1] Mark Asch, Marc Bocquet, and Maëlle Nodet. *Data assimilation: methods, algorithms, and applications*. SIAM, 2016.
- [2] L Bengtsson, M Ghil, and E Källén. *Dynamic Meteorology: Data Assimilation Methods*, volume 36. Springer, 1981.
- [3] G. Camerlengo. *Modal and Statistical Analysis of the Compressible Round Impinging Jet considering Turbulent Inflow, System Geometry and Cross-Flow Effects*. PhD thesis, Technische Universität Berlin, Berlin, 2023.
- [4] Geir Evensen. The ensemble kalman filter: Theoretical formulation and practical implementation. *Ocean dynamics*, 53:343–367, 2003.
- [5] J. J. P. Fernández. *The compressible starting jet: Fluid mechanics and acoustics*. PhD thesis, Technische Universität Berlin, 2018.
- [6] F Gaidzik, D Stucht, C Rolo, O Speck, D Thévenin, and G Janiga. Transient flow prediction in an idealized aneurysm geometry using data assimilation. *Computers in Biology and Medicine*, 115:103507, 2019.
- [7] M. Giles and N. Pierce. An introduction to the adjoint approach to design. *Flow, Turbulence and Combustion*, 2000.
- [8] Michael B. Giles and Niles A. Pierce. Adjoint equations in cfd: duality, boundary conditions and solution behaviour. 1997.
- [9] Alejandro Gronsksis, Dominique Heitz, and Étienne Mémin. Inflow and initial conditions for direct numerical simulation based on adjoint data assimilation. *Journal of Computational Physics*, 242:480–497, 06 2013.
- [10] William W Hager and Hongchao Zhang. A survey of nonlinear conjugate gradient methods. *Pacific journal of Optimization*, 2(1):35–58, 2006.
- [11] Thomas M Hamill and Chris Snyder. A hybrid ensemble kalman filter–3d variational analysis scheme. *Monthly Weather Review*, 128(8):2905–2919, 2000.
- [12] Rudolph Emil Kalman. A new approach to linear filtering and prediction problems. *Transactions of the ASME–Journal of Basic Engineering*, 82(Series D):35–45, 1960.
- [13] Leslie Kovasznay. Turbulence in supersonic flow. *J. Aero. Sci.*, 20(10):657–682, 1953.
- [14] M. Lemke. *Adjoint based data assimilation in compressible flows with application to pressure determination from PIV data*. PhD thesis, Technische Universität Berlin, Berlin, 2015.
- [15] Mathias Lemke, Julius Reiss, and Jörn Sesterhenn. Adjoint-based analysis of thermoacoustic coupling. In *AIP Conference Proceedings*, volume 1558, pages 2163–2166. American Institute of Physics, 2013.

- [16] Mathias Lemke, Julius Reiss, and Jörn Sesterhenn. Adjoint based optimisation of reactive compressible flows. *Combustion and Flame*, 161(10):2552–2564, 2014.
- [17] Mathias Lemke, Jan Schulze, and Joern Sesterhenn. Adjoint-based reconstruction of an entropy source by discrete temperature measurements. *International Journal of Computational Science and Engineering* 2, 9(5-6):526–537, 2014.
- [18] Mathias Lemke and Jörn Sesterhenn. Adjoint-based pressure determination from piv data in compressible flows—validation and assessment based on synthetic data. *European Journal of Mechanics-B/Fluids*, 58:29–38, 2016.
- [19] Mathias Lemke and Lewin Stein. Adjoint-based identification of sound sources for sound reinforcement and source localization. In *Fundamentals of High Lift for Future Civil Aircraft: Contributions to the Final Symposium of the Collaborative Research Center 880, December 17-18, 2019, Braunschweig, Germany*, pages 263–278. Springer, 2021.
- [20] Andrew C Lorenc. The potential of the ensemble kalman filter for nwp—a comparison with 4d-var. *Quarterly Journal of the Royal Meteorological Society: A journal of the atmospheric sciences, applied meteorology and physical oceanography*, 129(595):3183–3203, 2003.
- [21] Robert N Miller, Everett F Carter Jr, and Sally T Blue. Data assimilation into nonlinear stochastic models. *Tellus A*, 51(2):167–194, 1999.
- [22] Ionel M. Navon. *Data Assimilation for Numerical Weather Prediction: A Review*, pages 21–65. Springer Berlin Heidelberg, Berlin, Heidelberg, 2009.
- [23] Jorge Nocedal and Stephen J. Wright. *Numerical Optimization*. Springer, New York, NY, USA, 2e edition, 2006.
- [24] Juan José Peña Fernández and Jörn Sesterhenn. Compressible starting jet: pinch-off and vortex ring–trailing jet interaction. *Journal of Fluid Mechanics*, 817:560–589, 2017.
- [25] J Schulze and J Sesterhenn. Adjoint based noise minimization of a round supersonic jet. In *Journal of Physics: Conference Series*, volume 318, page 092005. IOP Publishing, 2011.
- [26] Jan Schulze and J Sesterhenn. Optimal control to reduce supersonic jet noise. In *New Results in Numerical and Experimental Fluid Mechanics VIII: Contributions to the 17th STAB/DGLR Symposium Berlin, Germany 2010*, pages 707–714. Springer, 2013.
- [27] Jörn Sesterhenn. A characteristic-type formulation of the navier–stokes equations for high order upwind schemes. *Computers and Fluids*, 30(1):37–67, 2000.
- [28] Lewin Stein, Florian Straube, Jörn Sesterhenn, Stefan Weinzierl, and Mathias Lemke. Adjoint-based optimization of sound reinforcement including non-uniform flow. *The Journal of the Acoustical Society of America*, 146(3):1774–1785, 2019.
- [29] Lewin Stein, Florian Straube, Stefan Weinzierl, and Mathias Lemke. Directional sound source modeling using the adjoint euler equations in a finite-difference time-domain approach. *The Journal of the Acoustical Society of America*, 148(5):3075–3085, 2020.
- [30] W. Sutherland. The viscosity of gases and molecular force. *The London, Edinburgh, and Dublin Philosophical Magazine and Journal of Science*, 36(223):507–531, 1893.
- [31] R. Wilke. *The Impinging Jet*. PhD thesis, Technische Universität Berlin, Berlin, 2017.

Abstract in lingua italiana

Viene eseguita un'analisi di osservabilità del metodo di assimilazione dei dati basato sull'operatore aggiunto applicato a un getto di avviamento comprimibile. In primo luogo, il sistema di assimilazione dei dati basato sull'aggiunto viene derivato e convalidato per un semplice problema di identificazione di una sorgente acustica. In secondo luogo, viene effettuata un'analisi di osservabilità dei modi di Kovasznay con l'intento di avere un punto di riferimento per le proprietà di osservabilità del metodo di assimilazione di dati derivato, applicato alle perturbazioni intorno a uno stato base. In terzo luogo, viene presentata l'assimilazione dei dati di un getto di avviamento comprimibile. I dati per l'assimilazione provengono da una DNS e sono utilizzati come input sperimentale sintetico. Viene valutata la capacità della procedura di assimilazione dei dati di trovare un buon fit dati due snapshots del flusso a diversi intervalli di tempo. Inoltre, viene eseguita un'analisi di osservabilità sistematica nel caso del getto iniziale. La capacità del metodo DA di adattarsi ai dati disponibili è valutata positivamente. Il caso particolare di applicazione utilizzato in questo lavoro ha presentato difficoltà nella ricostruzione di variabili non note.

Parole chiave: assimilazione di dati, flussi comprimibili, getti di avviamento, aggiunto delle equazioni di Navier-Stokes